Heterogeneous Catalysis Hot Paper

International Edition: DOI: 10.1002/anie.201511558
German Edition: DOI: 10.1002/ange.201511558

Nitrogen-Doped Ordered Mesoporous Carbon Supported Bimetallic PtCo Nanoparticles for Upgrading of Biophenolics

*Guang-Hui Wang, Zhengwen Cao, Dong Gu, Norbert Pfänder, Ann-Christin Swertz, Bernd Spliethoff, Hans-Josef Bongard, Claudia Weidenthaler, Wolfgang Schmidt, Roberto Rinaldi, and Ferdi Schüth**

Abstract: *Hydrodeoxygenation (HDO) is an attractive route for the upgrading of bio-oils produced from lignocellulose. Current catalysts require harsh conditions to effect HDO, decreasing the process efficiency in terms of energy and carbon balance. Herein we report a novel and facile method for synthesizing bimetallic PtCo nanoparticle catalysts (ca. 1.5 nm) highly dispersed in the framework of nitrogen-doped ordered mesoporous carbon (NOMC) for this reaction. We demonstrate that NOMC with either 2D hexagonal (p6m) or 3D cubic ($Im\bar{3}m$) structure can be easily synthesized by simply adjusting the polymerization temperature. We also demonstrate that PtCo/NOMC (metal loading: Pt 9.90 wt%; Co 3.31 wt%) is a highly effective catalyst for HDO of phenolic compounds and "real-world" biomass-derived phenolic streams. In the presence of PtCo/NOMC, full deoxygenation of phenolic compounds and a biomass-derived phenolic stream is achieved under conditions of low severity.*

Bio-oils are mixtures of highly functionalized oxygenates obtained by pyrolytic[1] or non-pyrolytic[2] processes performed on lignocellulose. An essential step in the utilization of bio-oils as a feedstock for the production of biofuels constitutes the catalytic upgrading, that is, the removal of oxygen-containing groups from the bio-oils (oxygen content: 30–50 wt%). This step improves the stability of the bio-oils, and increases the energy density, so that properties similar to those of conventional fossil, oil-based, transportation fuels are achieved.[3] Hydrodeoxygenation (HDO), a highly attractive route for upgrading of bio-oils, involves reactions of the bio-oil with hydrogen to produce hydrocarbons and water.[1] Many catalysts for HDO processes have been studied, and they include metals (e.g., Pt, Pd, Ru, Rh, Fe, Ni, Co), metal sulfides (e.g., CoMo- and NiMo-based sulfides), metal phosphides (e.g., Ni_2P and Co_2P), metal carbides (e.g., W_2C and Mo_2C), or related compounds.[4] Recently, we found that bimetallic PtCo nanoparticles (ca. 3.6 nm) in hollow carbon nanospheres show high activity for hydrogenolysis of 5-hydroxymethylfurfural to 2,5-dimethylfuran with 98% yield.[5] Such catalysts are capable of hydrodeoxygenating C=O and C−OH groups without the drawbacks associated with the use of acidic supports (i.e. the promotion of side reactions, e.g., dehydration, cracking, and polymerization; the polymerization reaction contributes to catalyst deactivation via formation of carbonaceous deposits on the metal particles).[4a,b] Therefore, we hypothesized that the bimetallic PtCo catalysts should also be conducive to efficient upgrading of biomass-derived phenolic streams.

To utilize the active PtCo components efficiently, one approach is to downsize the bimetallic PtCo nanoparticles and finely disperse them on supports. The supports should allow efficient mass transfer, and suppress sintering and loss of the active catalyst during the HDO process. Nitrogen-doped ordered mesoporous carbon (NOMC) meets these requirements as a result of a combination of properties, that is, ordered mesoporosity of the carbon (with narrow pore size distribution, interconnected mesopores, large pore volumes and surface areas) and a nitrogen-doped carbon framework (with improved basicity and enhanced π-donor capability).[6] However, synthesis of PtCo/NOMC with small size of the metal particles and high dispersion of the particles in a simple way is very challenging. Firstly, it is hard to synthesize NOMC via soft-templating with in situ nitrogen doping, which would be the simplest method with respect to materials synthesis, owing to the limited availability of suitable nitrogen-containing precursors.[6e] Therefore, it is desirable to find suitable precursors for synthesis of the NOMC with high nitrogen content and well-defined ordered structures. Secondly, introducing metal nanoparticles, especially bimetallic nanoparticles, into the ordered mesoporous structures with high dispersion and narrow particle size distribution has proven to be very challenging.[7] Herein, we report a simple method to synthesize bimetallic PtCo nanoparticles supported in the framework of NOMC with ultrafine dispersion and uniform particle size distribution (ca. 1.5 nm). We demonstrate that PtCo/NOMC shows outstanding catalytic performance in the upgrading of phenolic compounds and 'real-world" biomass-derived phenolic stream. In both cases, the oxygen content is nearly fully removed.

Our strategy for preparing NOMC and PtCo/NOMC is illustrated in Scheme 1. NOMC is synthesized by the soft-templating method using 3-aminophenol as both nitrogen and

[*] Dr. G.-H. Wang, Dr. Z. Cao, Dr. D. Gu, N. Pfänder, A.-C. Swertz, B. Spliethoff, H.-J. Bongard, Dr. C. Weidenthaler, Dr. W. Schmidt, Prof. Dr. F. Schüth
Max-Planck-Institut für Kohlenforschung
Kaiser-Wilhelm-Platz 1, 45470 Mülheim an der Ruhr (Germany)
E-mail: schueth@kofo.mpg.de
N. Pfänder
Max-Planck-Institut für Chemische Energiekonversion
Stiftstrasse 34–36, 45470 Mülheim an der Ruhr (Germany)
Dr. R. Rinaldi
Imperial College London, Department of Chemical Engineering
South Kensington Campus, London, SW7 2AZ (UK)

Supporting information for this article can be found under: http://dx.doi.org/10.1002/anie.201511558.

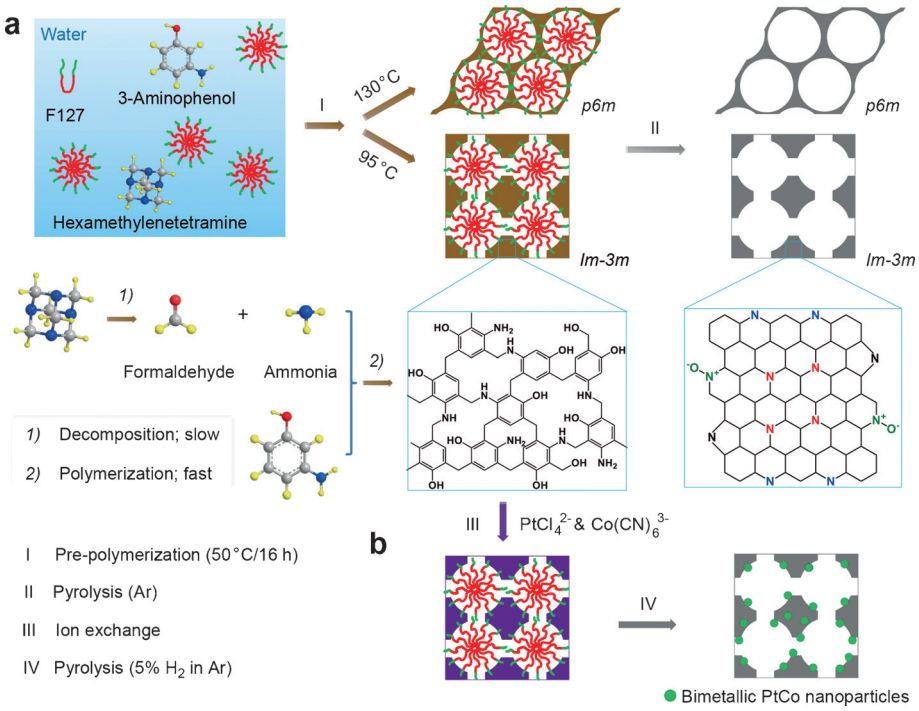

Scheme 1. Synthesis of a) NOMC and b) PtCo/NOMC.

carbon source. Theoretically, both the phenolic hydroxy group and amino group of 3-aminophenol have a strong interaction via hydrogen-bonding with the PEO moiety of F127 (poly(ethylene oxide)-poly(propylene oxide)-poly(ethylene oxide) triblock copolymer, EO106PO70EO106), which can induce the ordered assembly between 3-aminophenol/formaldehyde resin and F127.[8] However, the main problem using 3-aminophenol as the precursor is the too fast, uncontrolled polymerization of 3-aminophenol with formaldehyde, which hinders the formation of ordered mesoporous structures. In fact, on adding formaldehyde into a 3-aminophenol solution, the mixture turns opaque white (colloidal resin spheres formed) within 10 seconds even at room temperature, indicating rapid polymerization.[9] In the present system, hexamethylenetetramine (HMT) is used which can decompose into formaldehyde and ammonia (no polymerization occurred at room temperature). As the decomposition of HMT is temperature dependent, the polymerization rate can be thus efficiently controlled by adjusting the reaction temperature. Notably, depending on the reaction temperature, the selective formation of ordered mesostructured resin/F127 composites with either 2D hexagonal (*p6m*, NOMC-1 precursor) or 3D cubic ($Im\bar{3}m$, NOMC-2 precursor) symmetry can be achieved (Scheme 1 a). After carbonization at temperatures of 600 to 1000 °C (argon atmosphere), NOMC with high nitrogen content and well-defined ordered structures (*p6m* NOMC-1 and $Im\bar{3}m$ NOMC-2) can be obtained (Scheme 1 a), owing to the thermally highly stable resin/F127 composite framework with 3D-connected benzene rings.[10] Alternatively, both $PtCl_4^{2-}$ and $Co(CN)_6^{3-}$ ions can be introduced simultaneously into the resin/F127 composite by ion exchange. After pyrolysis under reductive condition (5 % H_2 in argon), PtCo/NOMC with ultrafine dispersion and uniform particle size distribution is produced (Scheme 1 b).

Low-angle powder X-ray diffraction (XRD) pattern of NOMC-1-600 (Figure 1 a) shows an intense diffraction peak and two weak peaks, which can be indexed as (10), (11), and (20) reflections associated with 2D hexagonal *p6m* symmetry.[11] The position of the intense (10) peak indicates a *d*-spacing of 11.1 nm, corresponding to a unit cell parameter of 12.8 nm. Transmission electron microscopy (TEM) images of NOMC-1-600 (Figure 1 b,c) viewed along the [001] and [110] directions, together with the scanning electron microscope (SEM) image (Figure 1 g), further confirm the hexagonal mesoporous structure. The cell parameter calculated from the TEM image is 12.4 nm, which is in

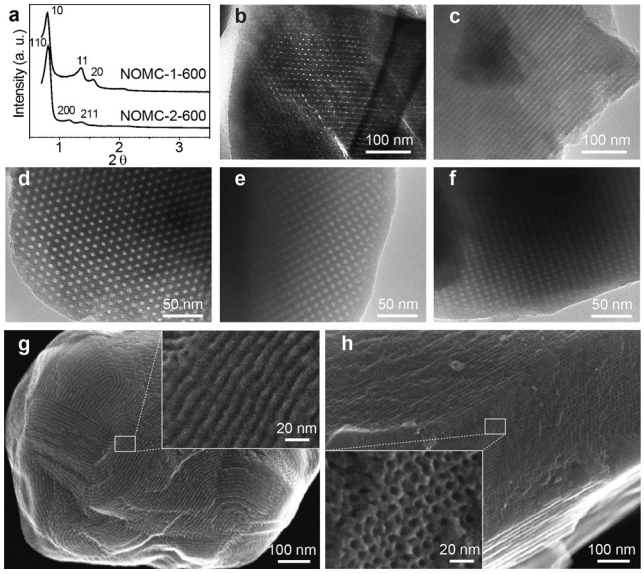

Figure 1. a) XRD patterns of NOMC-1-600 and NOMC-2-600. TEM images of NOMC-1-600 viewed in the b) [001] and c) [110] directions. TEM images of NOMC-2-600 viewed in the d) [111], e) [100], and f) [110] directions. SEM images of g) NOMC-1-600 and h) NOMC-2-600.

agreement with the value calculated from XRD data. Increasing the carbonization temperatures to 800 °C and 1000 °C, the XRD patterns (Supporting Information, Figure S1 a) are similar to that of NOMC-1-600, demonstrating the preservation of *p6m* symmetry and structure. As expected, the peak positions are shifted to higher angles,

indicating shrinkage of the carbon framework with elevated temperature (cell parameters decrease to 12.5 and 11.9 nm based on XRD data, Table S1). The XRD pattern of NOMC-2-600 (Figure 1a) also shows well-resolved reflections that can be indexed as (110), (200), and (211) reflections associated with body-centered cubic $Im\bar{3}m$ symmetry.[12] The cell parameter is estimated at 15.3 nm based on XRD data. TEM images (Figure 1d–f) show that NOMC-2-600 has a high degree of periodicity viewed from [111], [100], and [110] directions. The SEM image (Figure 1h) also shows a long-range order and large domains of interconnected cage-type pores in cubic 3D arrangement. This observation confirms the formation of a cubic mesoporous structure ($Im\bar{3}m$). The cell parameter calculated from TEM is 14.7 nm, in agreement with the value determined from XRD data. Also, the XRD patterns (Figure S1b) confirm that the cubic mesoporous structures are retained upon carbonization at 800 °C and 1000 °C. Also for NOMC-2, a shrinkage of the structure was observed at elevated temperature (cell parameters decrease to 14.4 nm for NOMC-2-800 and 14.0 nm for NOMC-2-1000 based on XRD data, Table S1).

The N_2 sorption isotherm of NOMC-1-600 (Figure S2a) shows a type-IV curve with type-H1 hysteresis loop, indicating a mesoporous structure with cylindrical channels.[11] BET surface area and the total pore volume are calculated to be 450 $m^2 g^{-1}$ and 0.26 $cm^3 g^{-1}$, respectively. The pore diameter is about 3.3 nm with a narrow pore size distribution (Figure S2b). Increasing the carbonization temperatures to 800 °C and 1000 °C, the isotherms (Figure S2a) still show typical type-IV curves, indicating the preservation of mesoporous structures. However, the adsorption and desorption branches are not closed, a phenomenon that is often observed for porous polymers and sometimes for porous carbons, and which is not yet fully understood. BET surface areas and the total pore volumes are decreased to 364 $m^2 g^{-1}$ and 0.22 $cm^3 g^{-1}$ for NOMC-1-800, and 254 $m^2 g^{-1}$ and 0.15 $cm^3 g^{-1}$ for NOMC-1-1000, respectively. The pore diameters for both NOMC-1-800 and NOMC-1-1000 are about 3.2 nm, which are similar to that of NOMC-1-600 (Figure S2b and Table S1). The N_2 sorption isotherm of NOMC-2-600 (Figure S2c) shows a type-IV curve with type-H2 hysteresis loop, which is typical for spherical pores with narrow pore windows.[13] NOMC-2-600 has a large BET surface area of 464 $m^2 g^{-1}$ and a pore volume of 0.30 $cm^3 g^{-1}$. The pore diameter is about 4.7 nm with a narrow pore size distribution (Figure S2d). The mesoporous structures are also preserved after carbonization at 800 °C and 1000 °C (Figure S2c). Similar as for NOMC-1, the desorption branches of NOMC-2-800 and NOMC-2-1000 do not meet the adsorption branches at low pressures. BET surface areas and the total pore volumes are 433 $m^2 g^{-1}$ and 0.28 $cm^3 g^{-1}$ for NOMC-2-800, and 400 $m^2 g^{-1}$ and 0.27 $cm^3 g^{-1}$ for NOMC-2-1000, respectively. Notably, the pore diameters remain at approximately 4.6 nm after carbonization at temperatures between 600 to 1000 °C (Figure S2d and Table S1).

The X-ray photoelectron spectrum (XPS) of NOMC-1-600 (Figure S3a) shows intense signals of carbon, nitrogen, and oxygen. In the N 1s region, the spectrum of NOMC-1-600 (Figure S3b) exhibits two peaks which can be attributed to pyridinic (398.4 eV) and pyrrolic nitrogen (400.5 eV).[14] Increasing the carbonization temperature to 800 and 1000 °C results in a N 1s spectra with five peaks, which can be assigned to nitride (397.9 eV), amine (399.1 eV), pyridonic nitrogen (400.8 eV), probably quaternary nitrogen (401.9 eV), and pyridine-*N*-oxide (403.3 eV;[15] Figure S3b). According to the elemental analysis by sample combustion, the amount of bulk nitrogen in NOMC-1-600 is 9.2 wt%. However, the total nitrogen content decreases to 7.8 wt% for NOMC-1-800 and 3.5 wt% for NOMC-1-1000, respectively (Table S1).

To introduce PtCo metal nanoparticles into NOMC with homogenous dispersion, the Pt and Co precursors were adsorbed into the polymer matrix (NOMC-2 precursor) first. Then, the polymer matrix was converted into NOMC-2 at 500 °C in a flow of 5% H_2 in Ar. During that treatment the bimetallic PtCo nanoparticles were formed with ultrafine dispersion and narrow particle size distribution. The majority of metal nanoparticles with diameters of about 1.5 nm were incorporated into the carbon frameworks (Figure 2a–c, Figure S4). Thus, they are firmly anchored to the carbon support

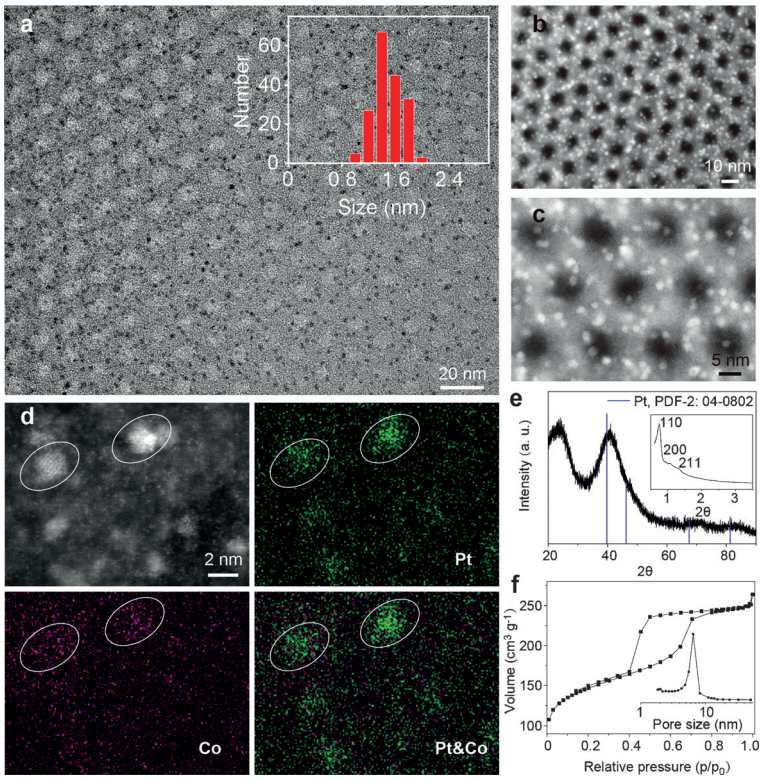

Figure 2. Structural characterization of PtCo/NOMC-2: a) TEM image. Inset: the particle size distribution of PtCo. b,c) STEM images. d) Elemental mappings (white ovals indicate the same particle in each panel). e) XRD pattern (positions of reflections for pure Pt marked by vertical lines). Inset: low-angle XRD pattern. f) N_2 sorption isotherm. Inset: pore size distribution.

which should improve their thermal stability during catalysis. EDX data (Figure S4) show that the sample contains Pt and Co with a molar ratio of Pt:Co of about 1:1.1. This is in agreement with data from atomic absorption spectrometry (AAS; 9.90 wt% Pt, 3.31 wt% Co; the corresponding molar ratio of Pt and Co is 1:1.1). Furthermore, according to the elemental mappings of Pt and Co (Figure 2d), the distributions of Pt and Co in the NOMC almost overlap with each other. In the XRD pattern (Figure 2e) the reflections are shifted to higher angles compared with those of pure Pt. This observation indicates that Co is very likely incorporated into the Pt *fcc* structure to form an alloy phase. In addition, the XRD reflections are very broad, further confirming the formation of small bimetallic PtCo nanoparticles. The low-angle XRD pattern (Figure 2e, inset) shows well-resolved reflections, indicating the presence of a cubic mesoporous structure after introduction of PtCo nanoparticles. The N_2 sorption isotherm of PtCo/NOMC-2 (Figure 2f) still shows a type-IV curve with type-H2 hysteresis loop, which further confirms the stability of the ordered mesoporous structure. BET surface area, pore volume and pore size of PtCo/NOMC-2 are 507 $m^2 g^{-1}$, 0.41 $cm^3 g^{-1}$ and 6.5 nm, respectively, which are larger than those for NOMC-2–600 without metal loading. This result can be attributed to the decomposition of carbon in the presence of Co or the lower pyrolysis temperature (500 °C). This finding has also been observed in a related synthesis for the generation of bimetallic PtCo nanoparticles encapsulated in hollow carbon spheres.[5]

The catalytic performance of PtCo/NOMC-2 was evaluated for HDO of phenolic compounds. First a blank reaction without added catalyst was carried out. In this test, the conversion of guaiacol was lower than 3% even after reaction for 24 h (Table S2, entry 1). Next, a commercial Pt/C catalyst, Pt/NOMC-2 and Co/NOMC-2 (Figure S5) were compared in the HDO of guaiacol under the same conditions. In the presence of commercial Pt/C, full conversion of guaiacol was achieved, but rendering an HDO degree of only 27% (Table S2, entry 2); the main products were methoxycyclohexanol (57%), cyclohexanol (33%), and cyclohexane (10%), indicating that the main reaction channel is the aromatic ring saturation. For Pt/NOMC-2, a 96% conversion of guaiacol was obtained, affording a 50% HDO degree (Table S2, entry 3); the main products were methoxycyclohexanol (4%), cyclohexanol (79%) and cyclohexane (4%). These results indicate that monometallic Pt nanoparticles possess high hydrogenation activity but low deoxygenation activity. In turn, Co/NOMC-2 led to a 21% conversion of guaiacol and 31% HDO degree (Table S2, entry 4). However, when using PtCo/NOMC-2 as the catalyst, full conversion of guaiacol into cyclohexane (selectivity > 99%) was achieved (Table S2, entry 5). Guaiacol thus seems to undergo a hydrogenation-deoxygenation process under the reaction conditions over PtCo/NOMC-2 (Figure S6). The high HDO activity of PtCo/NOMC-2 was further confirmed by experiments using other phenolic compounds (Table S2, entries 6 and 7). The selectivity for the alkanes was always > 99%, which gave an overall HDO degree of > 99% at full conversion. Altogether, these results demonstrate a synergism between Pt and Co caused by the electronic interaction between Pt and Co in the bimetallic PtCo nanoparticles.[5] Notably, compared with results reported in recent literature (Table S3), the HDO activity of PtCo/NOMC-2 is higher than most acid-free or acidic support-free catalysts, and comparable to catalysts containing acids or acidic supports.

Recycling tests of PtCo/NOMC-2 for HDO of guaiacol were carried out at 573 K under 10 MPa H_2 for 1 h. The guaiacol conversion slightly decreased from 100% in cycle 1 to 94% in cycle 5 (Figure S7). However, the HDO activity gradually decreased after three runs, as indicated by the increased cyclohexanol formation in conjunction with the decrease in the cyclohexane selectivity (Figure S7, run 4 and 5). This result may be associated with the leaching of Co from the surface of the bimetallic PtCo nanoparticles during the recycling tests (Figure S8). Accordingly, a hot filtration test was also performed. After removal of the solid catalyst, the reaction in the filtrate did not proceed (Table S2, entries 8–10), indicating that no catalytically active species are present in the filtrate. However, trace amounts of Pt (8.3 ppm) and Co (0.8 ppm) were still detected (AAS) in the filtrate. These results indicate that the catalytic effect in this system results from the PtCo nanoparticles on the support and not from leached metal species.

We further applied the PtCo/NOMC-2 catalyst for HDO of a lignin-derived non-pyrolytic bio-oil, which had been obtained from early-stage catalytic conversion of lignin (ECCL)[16] through hydrogen transfer reaction in the presence of Raney Ni and 2-propanol.[2] Through this approach, lignin is depolymerized directly after its extraction from plant biomass in a one-pot process. Advantageously, in its composition, the lignin oil stream mostly comprises monocyclic phenols and, to a lesser extent, alcohols and phenolic oligomers. Moreover, as ECCL directly reduces carbonyl functionalities (associated with ketones and aldehydes), the lignin oil stream is obtained as a thermally stable stream. Therefore, the "new" lignin stream clearly exhibits properties that are conducive to downstream using highly active, tailor-made nanocatalysts as these reported herein.

The main components in the as-obtained non-pyrolytic bio-oil (elemental analysis: C 57.1%; H 7.9%; O 35.0% by difference) are phenolics derived from lignin (Figure 3a). After HDO of the lignin-oil over PtCo/NOMC-2, the main products are cycloalkanes (Figure 3b). Remarkably, almost no oxygen-containing compounds were detected by GC × GC-MS analysis. The HSQC spectrum of the product after HDO (isolated at 313 K under 50 mbar) clearly shows only the characteristic signals of aliphatic C(sp^3)-H; the oxygen functionalities in the non-pyrolytic bio-oil were almost fully removed (Figure S9). The elemental analysis shows that the sum of C and H in the isolated product is up to 99% (C 84.9%; H 14.1%). Therefore, PtCo/NOMC-2 is indeed an effective catalyst for HDO of complex phenolic streams derived from native lignin without added acid co-catalysts or acidic supports. The deoxygenated product mixture can potentially be processed in conventional oil refineries, and therefore, valorizing residual lignin streams obtained from cellulosic bio-ethanol.

In summary, we have developed a soft-templating pathway for the synthesis of NOMC using 3-aminophenol as both

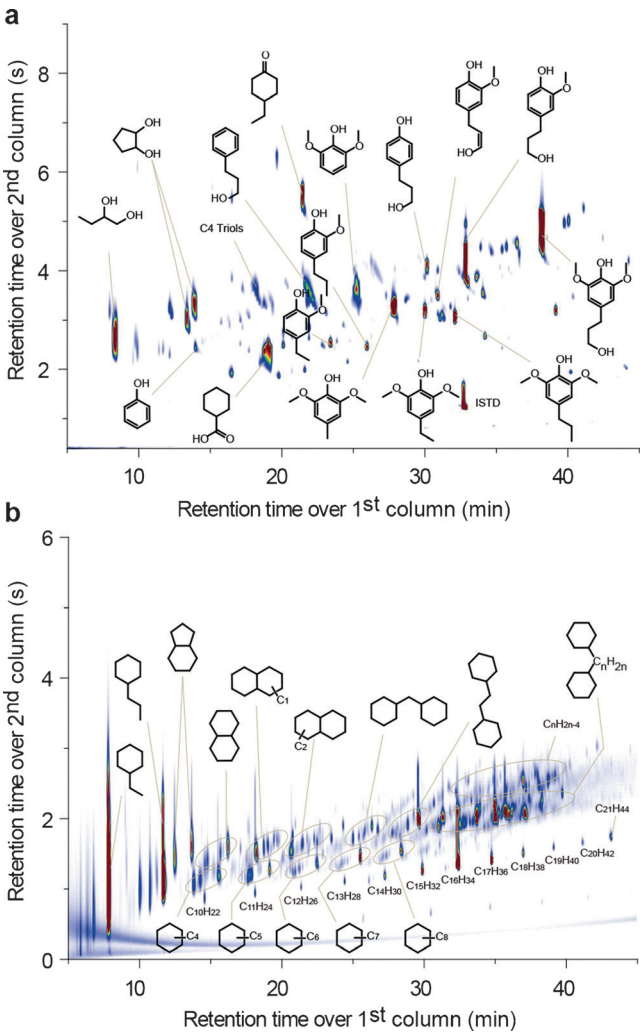

Figure 3. GC×GC-MS analysis of lignin-derived non-pyrolytic bio-oil before (a) and after (b) HDO over PtCo/NOMC-2. Reaction conditions: bio-oil (200 mg), *n*-hexadecane (GC internal standard, 0.4 mmol), catalyst (200 mg), and *n*-hexane (solvent, 5 mL), 10 MPa (573 K, constant), 573 K for 12 h.

carbon and nitrogen source. NOMC with *p6m* and $Im\bar{3}m$ mesostructured symmetries were successfully synthesized by simply changing the polymerization temperature. The nitrogen content of NOMC can be adjusted from approximately 9.2 wt% to approximately 3.5 wt% by increasing the carbonization temperature from 600 °C to 1000 °C. Moreover, the structures of NOMC are stable even upon carbonization at 1000 °C. Notably, bimetallic PtCo nanoparticles with diameters of around 1.5 nm were successfully introduced into the NOMC framework with ultrafine dispersion and uniform particle size distribution. The loadings of Pt and Co are 9.90 wt% and 3.31 wt%, respectively. The PtCo/NOMC shows outstanding catalytic performance in the HDO of phenolic compounds and complex "real-world" phenolic mixtures. The conversion of lignin oil obtained by ECCL produced cycloalkanes; the oxygen content was nearly fully removed. Such a lignin product mixture comprising cycloalkanes could already find uses as drop-in fuels or as performance-enhancer of synthetic fuels produced by the Fischer–Tropsch process.

Acknowledgements

This work was conducted in the framework of the ERC Advanced Grant project "POLYCAT" and the CASCATBEL project funded by the European Commission (Grant Agreement No. 604307). R.R. is grateful to the funding provided by Alexander von Humboldt Foundation (Sofja Kovalevskaja Award 2010). This work was performed as part of the Cluster of Excellence "Tailor-Made Fuels from Biomass", which is funded by the Excellence Initiative by the German federal and state governments to promote science and research at German universities. We thank Mr. Markus Kochius for NMR tests.

Keywords: bimetallic nanoparticles · biomass · hydrodeoxygenation · mesoporous materials · phenols

How to cite: *Angew. Chem. Int. Ed.* **2016**, *55*, 8850–8855
Angew. Chem. **2016**, *128*, 8996–9001

[1] G. W. Huber, S. Iborra, A. Corma, *Chem. Rev.* **2006**, *106*, 4044.
[2] P. Ferrini, R. Rinaldi, *Angew. Chem. Int. Ed.* **2014**, *53*, 8634; *Angew. Chem.* **2014**, *126*, 8778.
[3] a) J. Zakzeski, P. C. A. Bruijnincx, A. L. Jongerius, B. M. Weckhuysen, *Chem. Rev.* **2010**, *110*, 3552; b) R. K. Sharma, N. N. Bakhshi, *Energy Fuels* **1993**, *7*, 306; c) E. Furimsky, *Appl. Catal. A* **2000**, *199*, 147.
[4] a) P. M. Mortensen, J. D. Grunwaldt, P. A. Jensen, K. G. Knudsen, A. D. Jensen, *Appl. Catal. A* **2011**, *407*, 1; b) M. Saidi, F. Samimi, D. Karimipourfard, T. Nimmanwudipong, B. C. Gates, M. R. Rahimpour, *Energy Environ. Sci.* **2014**, *7*, 103; c) D. A. Ruddy, J. A. Schaidle, J. R. Ferrell, J. Wang, L. Moens, J. E. Hensley, *Green Chem.* **2014**, *16*, 454; d) H. M. Wang, J. Male, Y. Wang, *ACS Catal.* **2013**, *3*, 1047; e) K. L. Li, R. J. Wang, J. X. Chen, *Energy Fuels* **2011**, *25*, 854; f) N. Ji, M. Y. Zheng, A. Q. Wang, T. Zhang, J. G. G. Chen, *ChemSusChem* **2012**, *5*, 939; g) C. Zhao, J. A. Lercher, *ChemCatChem* **2012**, *4*, 64; h) C. R. Lee, J. S. Yoon, Y. W. Suh, J. W. Choi, J. M. Ha, D. J. Suh, Y. K. Park, *Catal. Commun.* **2012**, *17*, 54; i) D. Y. Hong, S. J. Miller, P. K. Agrawal, C. W. Jones, *Chem. Commun.* **2010**, *46*, 1038; j) T. Nimmanwudipong, R. C. Runnebaum, D. E. Block, B. C. Gates, *Energy Fuels* **2011**, *25*, 3417; k) X. Wang, R. Rinaldi, *Catal. Today* **2016**, *269*, 48.
[5] G. H. Wang, J. Hilgert, F. H. Richter, F. Wang, H. J. Bongard, B. Spliethoff, C. Weidenthaler, F. Schüth, *Nat. Mater.* **2014**, *13*, 294.
[6] a) X. Jin, V. V. Balasubramanian, S. T. Selvan, D. P. Sawant, M. A. Chari, G. Q. Lu, A. Vinu, *Angew. Chem. Int. Ed.* **2009**, *48*, 7884; *Angew. Chem.* **2009**, *121*, 8024; b) L. Liu, Q. F. Deng, T. Y. Ma, X. Z. Lin, X. X. Hou, Y. P. Liu, Z. Y. Yuan, *J. Mater. Chem.* **2011**, *21*, 16001; c) T. Y. Ma, L. Liu, Z. Y. Yuan, *Chem. Soc. Rev.* **2013**, *42*, 3977; d) W. Z. Shen, W. B. Fan, *J. Mater. Chem. A* **2013**, *1*, 999; e) X. Q. Wang, C. G. Liu, D. Neff, P. F. Fulvio, R. T. Mayes, A. Zhamu, Q. Fang, G. R. Chen, H. M. Meyer, B. Z. Jang, S. Dai, *J. Mater. Chem. A* **2013**, *1*, 7920; f) J. Wei, D. D. Zhou, Z. K. Sun, Y. H. Deng, Y. Y. Xia, D. Y. Zhao, *Adv. Funct. Mater.* **2013**, *23*, 2322; g) P. F. Zhang, Y. T. Gong, H. R. Li, Z. R. Chen, Y. Wang, *Nat. Commun.* **2013**, *4*, 1593; h) D. D. Zhou, W. Y. Li, X. L. Dong, Y. G. Wang, C. X. Wang, Y. Y. Xia, *J. Mater. Chem. A* **2013**, *1*, 8488; i) X. Q. Wang, J. S. Lee, Q. Zhu, J. Liu, Y. Wang, S. Dai, *Chem. Mater.* **2010**, *22*, 2178; j) J. H. Yu, M. Y. Guo, F.

Muhammad, A. F. Wang, G. L. Yu, H. P. Ma, G. S. Zhu, *Microporous Mesoporous Mater.* **2014**, *190*, 117; k) J. Y. Yu, M. Y. Guo, F. Muhammad, A. F. Wang, F. Zhang, Q. Li, G. S. Zhu, *Carbon* **2014**, *69*, 502; l) Y. D. Xia, R. Mokaya, *Adv. Mater.* **2004**, *16*, 1553; m) M. Kruk, B. Dufour, E. B. Celer, T. Kowalewski, M. Jaroniec, K. Matyjaszewski, *J. Phys. Chem. B* **2005**, *109*, 9216; n) P. F. Fulvio, M. Jaroniec, C. D. Liang, S. Dai, *J. Phys. Chem. C* **2008**, *112*, 13126.

[7] X. L. Ji, K. T. Lee, R. Holden, L. Zhang, J. J. Zhang, G. A. Botton, M. Couillard, L. F. Nazar, *Nat. Chem.* **2010**, *2*, 286.

[8] J. Wang, H. Y. Liu, X. M. Gu, H. H. Wang, D. S. Su, *Chem. Commun.* **2014**, *50*, 9182.

[9] J. M. Zhao, W. X. Niu, L. Zhang, H. R. Cai, M. Y. Han, Y. L. Yuan, S. Majeed, S. Anjum, G. B. Xu, *Macromolecules* **2013**, *46*, 140.

[10] Y. Meng, D. Gu, F. Q. Zhang, Y. F. Shi, H. F. Yang, Z. Li, C. Z. Yu, B. Tu, D. Y. Zhao, *Angew. Chem. Int. Ed.* **2005**, *44*, 7053; *Angew. Chem.* **2005**, *117*, 7215.

[11] D. Y. Zhao, J. L. Feng, Q. S. Huo, N. Melosh, G. H. Fredrickson, B. F. Chmelka, G. D. Stucky, *Science* **1998**, *279*, 548.

[12] D. Y. Zhao, Q. S. Huo, J. L. Feng, B. F. Chmelka, G. D. Stucky, *J. Am. Chem. Soc.* **1998**, *120*, 6024.

[13] J. R. Matos, M. Kruk, L. P. Mercuri, M. Jaroniec, L. Zhao, T. Kamiyama, O. Terasaki, T. J. Pinnavaia, Y. Liu, *J. Am. Chem. Soc.* **2003**, *125*, 821.

[14] J. R. Pels, F. Kapteijn, J. A. Moulijn, Q. Zhu, K. M. Thomas, *Carbon* **1995**, *33*, 1641.

[15] K. Artyushkova, B. Kiefer, B. Halevi, A. Knop-Gericke, R. Schlögl, P. Atanassov, *Chem. Commun.* **2013**, *49*, 2539.

[16] R. Rinaldi, R. Jastrzebski, M. T. Clough, J. Ralph, M. Kennema, P. C. A. Bruijnincx, B. M. Weckhuysen, *Angew. Chem. Int. Ed.* **2016**, *55*, DOI: 10.1002/anie.201510351; *Angew. Chem.* **2016**, *128*, DOI: 10.1002/ange.201510351.

Received: December 12, 2015
Revised: February 28, 2016
Published online: June 13, 2016

